Blood Pool Agent Contrast-Enhanced MRA: Level-Set Based Artery-Vein Separation

Cornelis M. van Bemmel[a], Luuk Spreeuwers[a], Bert Verdonck[b],
Max A. Viergever[a], Wiro J. Niessen[a]

[a] Images Sciences Institute, Utrecht, The Netherlands
[b] Philips Medical Systems, Best, The Netherlands

ABSTRACT

Blood pool agents (BPAs) for contrast-enhanced magnetic resonance angiography (CE-MRA) allow prolonged imaging times for higher contrast and resolution by imaging during the steady state when the contrast agent is distributed through the complete vascular system. However, simultaneous arterial and venous enhancement hampers interpretation. It is shown that venous and arterial segmentation in this equilibrium phase can be achieved if the central arterial axis (CAA) and central venous axis (CVA) are known. Since the CAA cannot straightforwardly be obtained from the steady-state data, images acquired during the first pass of the contrast agent can be utilized to determine the CAA with minimal user initialization. Utilizing the CAA to provide a rough arterial segmentation, the CVA can subsequently be determined from the steady-state dataset. The final segmentations of the arteries and veins are achieved by simultaneously evolving two level-sets in the steady-state dataset starting from the CAA and CVA.

Keywords: Blood pool agent, contrast-enhanced MRA, segmentation.

1. INTRODUCTION

Blood pool agents for CE-MRA have a prolonged intra-vascular half-life and provide strong T1-relaxation even at low resolution.[1] Therefore, these agents allow imaging in the steady state, thus providing longer time windows for image acquisition, which can be advantageous if high contrast and/or resolution is required and a large anatomical region needs to be covered.[2] However, an important drawback of imaging in the steady-state is the simultaneous enhancement of arteries and veins, which hampers the interpretation of the steady-state data (see Figure 1).

Several artery-vein separation techniques have been proposed. Some approaches, *e.g.*[3–6] aim at separating arteries from veins during the acquisition stage. Phase contrast (PC) techniques[3,4] are flow-dependent and rely on the difference in blood flow direction in arteries and veins. Therefore, these techniques are only suitable for situations where the blood flow direction in arteries and veins is opposite. Wang *et al.* discriminate arteries from veins depending on the oxygenation level.[5] This flow-independent method relies on the BOLD (blood oxygenation level-dependent)-effect and is limited due to a sometimes higher oxygen-level in the veins than expected. Mazaheri *et al.* characterize each pixel as arterial, venous, or unenhanced background tissue during the first pass of the contrast agent using a time-resolved acquisition scheme.[6] However, the period in which the venous uptake lags the arterial uptake is very critical. Numerous articles have addressed the issue of vessel visualization and segmentation, *e.g.*[7–13] but only few have addressed the issue of artery-vein separation.[14–17] Bock *et al.* propose a method for artery-vein separation based on the difference in temporal enhancement kinetics of arterial and venous vascular signal in 3D MR angiograms of the lung.[14] Niessen *et al.* improved arterial visualization by suppressing the major overlapping veins in maximum intensity projections (MIP).[15]

Further author information: (Send correspondence to C.M. van Bemmel)
[a] E-mail: {kees, luuk, max, wiro}@isi.uu.nl, Telephone: +31 30 250.7772, Address: University Medical Center, Image Sciences Institute, Heidelberglaan 100, rm. E 01.334, NL-3584CX Utrecht, The Netherlands.
[b] E-mail: bert.verdonck@philips.com, Telephone: +31 40 276.2456, Address: Philips Medical Systems, EasyVision AD, PO Box 10.000, NL-5680DA Best, The Netherlands.

This visualization technique is only applicable for larger overlapping veins. Sonka *et al.* show the feasibility of artery-vein separation using a graph-search approach.[16] The most extensive work on artery-vein separation has been reported by Lei *et al.* who use the principle of fuzzy connectedness.[17, 18] First, all vascular structures are segmented from the background. Secondly, arteries are separated within this entire vessel structure from veins via an iterative fuzzy-connectedness procedure. Promising results have been reported on a large number of datasets. However, the authors acknowledge that validation is still required to assure that the results can clinically be used.

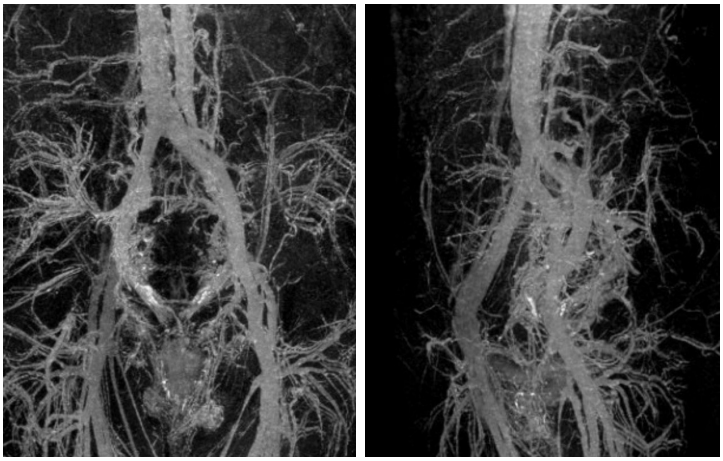

Figure 1. Maximum Intensity Projections (MIP) of a dataset acquired during the steady state (left posteroanterior, right oblique). Simultaneous enhancement of arteries and veins hampers interpretation.

In this paper a method for artery-vein separation is presented that is based on the level-set approach using the central arterial axis (CAA) and central venous axis (CVA), which are used for initializing two level-sets that simultaneously capture the arterial and venous vessel structure, respectively. Since the CAA cannot straightforwardly be determined from the steady-state dataset, information from the arteriogram acquired during the first pass of the contrast agent can be used to find the CAA.

2. METHODOLOGY

Our method uses the CAA and CVA as initializations for level-set based separation of the arteries and veins. Figure 2 shows a flow-diagram outlining the key steps in our approach. If a first-pass dataset is available, the CAA is derived semi-automatically from it.[19] This CAA is transferred to the steady-state dataset. In case of patient motion between the first-pass and steady-state acquisition, the datasets are registered prior to warping the paths obtained in the first-pass dataset to the steady-state dataset. This part of our proposed methodology is reflected by the shaded part of the flow-diagram. If no first-pass dataset is available, the CAA is outlined by an observer in the steady-state dataset. The remaining part of our methodology is the same. In order to determine the CVA, the major arterial part of the vasculature is removed by segmentation. Once the CAA and CVA are known, the arteries and veins, that are seeded by these axes, are segmented.

In Section 2.1 we describe the techniques employed for semi-automatic determination of a central vessel axis. Section 2.2 details the registration of the first-pass dataset to the steady-state dataset, and in Section 2.3 the separation of the arteries and veins is described.

2.1. Central Axis Determination

To find the central axis of an elongated structure (such as a vessel), we use a filter to enhance vessel-like structures. The reciprocal output of this filtering process (Section 2.1.1) is used for estimation of a minimum-cost path between user-defined points (Section 2.1.2).

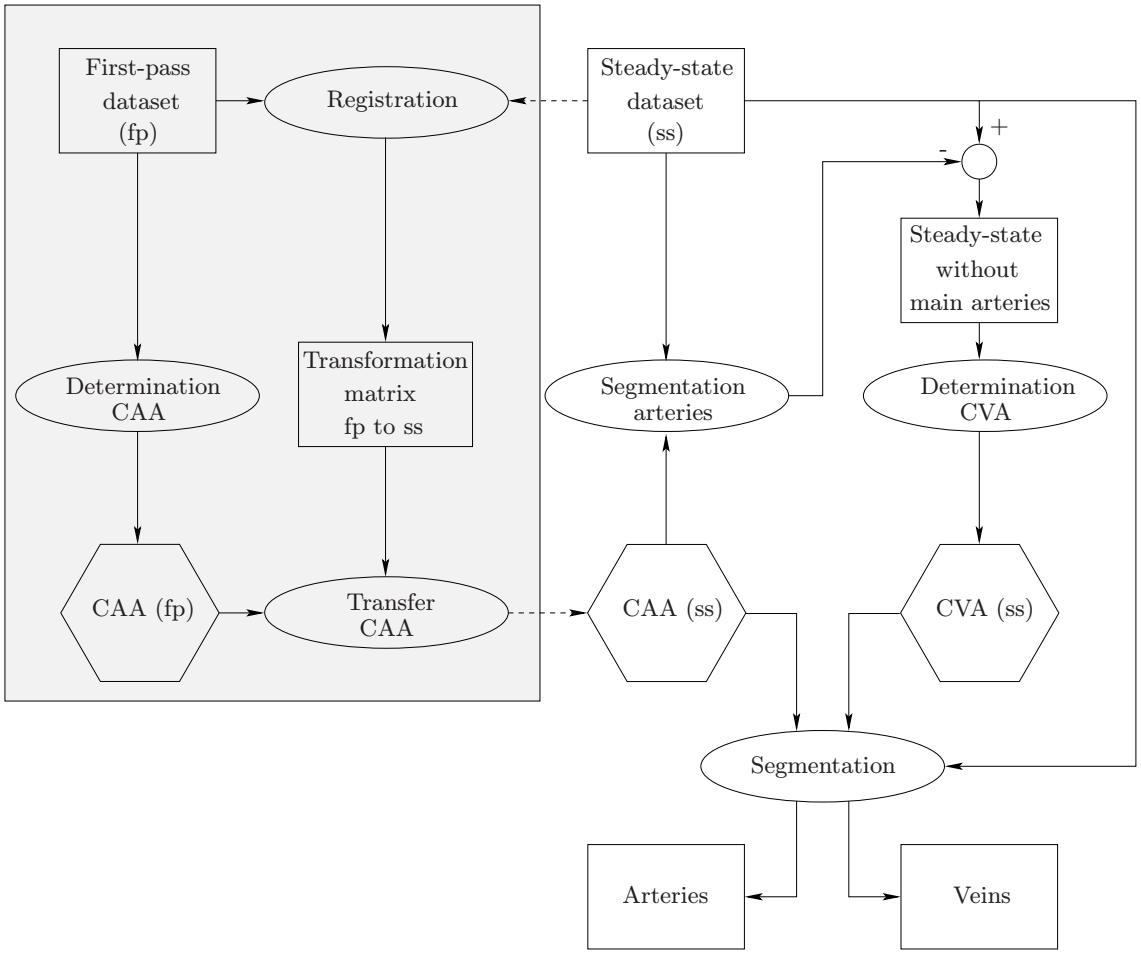

Figure 2: Overall block diagram of the proposed method.

2.1.1. Vessel-Enhancement

To determine the likeliness of a voxel to be part of a tubular structure, a filter is employed which analyzes the local second-order image structure.[11] The local image structure of an image L in the neighbourhood of a point $\mathbf{x}_0$ can be described with the Taylor expansion:

$$L(\mathbf{x}_0 + \delta\mathbf{x}_0, \sigma) \approx L(\mathbf{x}_0, \sigma) + \delta\mathbf{x}_0^T \nabla_{0,\sigma} + \delta\mathbf{x}_0^T \mathcal{H}_{0,\sigma} \delta\mathbf{x}_0, \tag{1}$$

where $\nabla_{0,\sigma}$ and $\mathcal{H}_{0,\sigma}$ are the gradient vector and Hessian matrix of the image computed in $\mathbf{x}_0$ at scale σ, respectively.

The Hessian matrix at a given voxel $\mathbf{x}$ is defined as:

$$\mathcal{H}(\mathbf{x}, \sigma) = \begin{bmatrix} L_{xx}(\mathbf{x}, \sigma) & L_{xy}(\mathbf{x}, \sigma) & L_{xz}(\mathbf{x}, \sigma) \\ L_{yx}(\mathbf{x}, \sigma) & L_{yy}(\mathbf{x}, \sigma) & L_{yz}(\mathbf{x}, \sigma) \\ L_{zx}(\mathbf{x}, \sigma) & L_{zy}(\mathbf{x}, \sigma) & L_{zz}(\mathbf{x}, \sigma) \end{bmatrix}, \tag{2}$$

where $L_{\xi_1\xi_2}(\mathbf{x}, \sigma)$ denote regularized derivatives of the image $L(\mathbf{x})$, which are obtained by convolving the image

with the derivatives of the Gaussian kernel at scale σ:

$$L_{\xi_1\xi_2}(\mathbf{x},\sigma) \triangleq \sigma^2 \frac{\partial^2 G(\mathbf{x},\sigma)}{\partial\xi_1\partial\xi_2} * L(\mathbf{x}) \tag{3}$$

$$G(\mathbf{x},\sigma) \triangleq \frac{1}{\sqrt{(2\pi\sigma^2)^3}} e^{-\frac{\|\mathbf{x}\|^2}{2\sigma^2}} \tag{4}$$

The principal directions in which the local second-order structure of the image can be decomposed are obtained by eigenvalue analysis of the Hessian matrix. Let $\lambda_{\sigma,k}$ denote the ordered eigenvalues corresponding to the k-th normalized eigenvector $\hat{\mathbf{u}}_{\sigma,k}$, *i.e.* $|\lambda_{\sigma,1}| \leq |\lambda_{\sigma,2}| \leq |\lambda_{\sigma,3}|$. The eigenvectors $\hat{\mathbf{u}}_{\sigma,k}$ compose three orthonormal directions: $\hat{\mathbf{u}}_1$ indicates the direction along the vessel (minimum intensity variation), $\hat{\mathbf{u}}_2$, and $\hat{\mathbf{u}}_3$ form a base of the orthogonal plane.

In order to estimate the likeliness that a voxel belongs to a vessel -from an analysis of the eigenvalues-, two geometric ratios ($\mathcal{R}_A$ and $\mathcal{R}_B$), and a measure for distinguishing background voxels from vessel voxels ($\mathcal{S}$) are introduced:

$$\mathcal{R}_A \triangleq \frac{|\lambda_2|}{|\lambda_3|}\ , \tag{5}$$

$$\mathcal{R}_B \triangleq \frac{|\lambda_1|}{\sqrt{|\lambda_2\lambda_3|}}\ , \tag{6}$$

$$\mathcal{S} \triangleq \|\mathcal{H}\|_F = \sqrt{\sum_j \lambda_j^2}\ . \tag{7}$$

The ratio $\mathcal{R}_A$ is essential for distinguishing between plate-like and line-like structures. The ratio $\mathcal{R}_B$ accounts for the deviation from a blob-like structure. $\mathcal{S}$ is a measure of "second-order structureness", and will be low in the background where no structure is present. In regions with high contrast compared to the background, the norm will become larger since at least one of the eigenvalues will be large.

Since in CE-MRA vessels give higher signals than the background, the output of the vessel-enhancement filter[11] in $\mathbf{x}$ at a single scale, σ, is therefore defined as:

$$\mathcal{V}(\mathbf{x},\sigma) \triangleq \begin{cases} 0 & \text{if } \lambda_2 > 0 \text{ or } \lambda_3 > 0, \\ (1 - e^{-\frac{1}{2}(\frac{\mathcal{R}_A}{\alpha})^2}) e^{-\frac{1}{2}(\frac{\mathcal{R}_B}{\beta})^2} (1 - e^{-\frac{1}{2}(\frac{\mathcal{S}}{\gamma})^2}) & \text{otherwise.} \end{cases} \tag{8}$$

The parameters α, β, and γ tune the sensitivity of the filter to deviations in $\mathcal{R}_A$, $\mathcal{R}_B$, and $\mathcal{S}$ relative to the ideal behavior for a line structure. Equation 8 implicitely states that the filter response is a function of the scale at which the Gaussian derivatives are computed. The filter is applied at multiple scales that span the range of expected vessel-widths according to the imaged anatomy. In order to provide a unique filter output for each voxel, the multiple scale outputs undergo a *scale selection* procedure, *i.e.* the maximum filter response across the scales is selected:

$$\mathcal{V}(\mathbf{x}) = \max_{\sigma_{min} \leq \sigma \leq \sigma_{max}} \mathcal{V}(\mathbf{x},\sigma). \tag{9}$$

In this way, different vessel sizes will be detected at their corresponding scales and both small and large vessels will be captured with the same scheme. When filtering data in order to enhance vessel-like structures, two outputs are generated. The first output is the vessel-enhanced image containing the maximal output of Equation 9 for each voxel. The second output is the scale-image containing for each voxel that scale at which the maximal output was found.

2.1.2. Minimum-Cost Path as an Estimation of the Central Axis

The central axis is estimated by finding the minimum-cost path[20,21] between user-defined points. In this approach, the image is treated as a grid of nodes, each with a 26-neighborhood. The transition costs of

traveling from node n to its neighbor n' is given by the arc-costs $a(n,n')$, which is defined as the reciprocal output of the vesselness filter, see Equation 9. The central axis between user-defined points is determined using a bi-directional search. In uni-directional algorithms, the search proceeds from the starting node forward until the goal node is encountered. In a bi-directional search the number of evaluations is reduced by starting a search-tree from both the starting node and the goal node simultaneously; the search-process ends when the two fronts meet. Costs are normalized with respect to the length in order to cope with diagonal transitions and (possible) anisotropic voxels. The search process can be understood as the propagation of a wavefront, where the speed is largest if the front is inside a vessel-like region. Since this minimum-cost path algorithm is voxel-based, the path is blurred to obtain a smooth estimate of the central axis. The accuracy of the CA with respect to manual tracings has been demonstrated in.[19]

2.2. Registration

To correct for possible patient motion between acquisition of the first-pass and steady-state dataset, the first-pass dataset is rigidly registered to the steady-state dataset. Alignment is achieved by maximizing the mutual information.[22,23] The MI-registration criterion states that two images are geometrically aligned by the transformation $T^\star$ for which $I(u(\mathbf{x}), v(T(\mathbf{x})))$ is maximal:

$$T^\star = \arg\{\max_T(I(u(\mathbf{x}), v(T(\mathbf{x}))))\}, \tag{10}$$

where the mutual information, I, is defined in terms of entropy and is a measure of variability:

$$I(u(\mathbf{x}), v(T(\mathbf{x}))) = h(u(\mathbf{x})) + h(v(T(\mathbf{x}))) - h(u(\mathbf{x}), v(T(\mathbf{x}))). \tag{11}$$

Here $h(.)$ is the entropy and is defined for one variable $\mathbf{x}$ as:

$$h(\mathbf{x}) \triangleq -\int p(\mathbf{x}) \ln p(\mathbf{x}) d\mathbf{x}. \tag{12}$$

The obtained transformation matrix $T^\star$ is applied to the minimum-cost path found in the first-pass dataset to obtain an estimate of the CAA in the steady-state dataset.

2.3. Vessel Separation

In Section 2.3.1 we describe the level-set technique as formulated by Osher[24] and Sethian[25,26] applied to vessel segmentation. In Section 2.3.2 we describe which features we applied for separation of the arteries and veins.

2.3.1. Artery-Vein Separation using Level-Sets: Interface

Arterial and venous vessel separation is achieved via level-set techniques in which the CAA and CVA serve as initializations for two competitive fronts. The separation can be regarded as the evolution of two fronts, or interfaces, towards the boundaries of the arterial and venous vasculature. Rather than evolving an interface itself, it is represented by the zero level-set of a higher dimensional function. To formalize these notions, let $\Gamma(t)$ denote a time-dependent closed (N-1)-dimensional hyper-surface. This interface evolves in its normal direction:

$$\Gamma_t(t) = F \cdot \vec{N}, \tag{13}$$

where F denotes the speed function and $\vec{N}$ the normal vector to the hyper-surface, pointing outwards.

Now, an N-dimensional function $\phi(t)$ is defined such that $[\phi(t) = 0] = \Gamma(t)$, *i.e.* $\Gamma(t)$ is represented by the zero level-set of $\phi(t)$ at all times. It can easily be shown that if $\Gamma(t)$ evolves according Equation 13, the evolution of $\phi(t)$ is given by[26]:

$$\phi_t(t) + F|\nabla\phi(t)| = 0. \tag{14}$$

So, the evolution of the zero level-set of $\phi(t)$ equals the evolution of $\Gamma(t)$. Therefore, in level-set based image segmentation, the evolution of $\Gamma(t)$ is implicitly defined by evolving $\phi(t)$. This approach has the advantage that

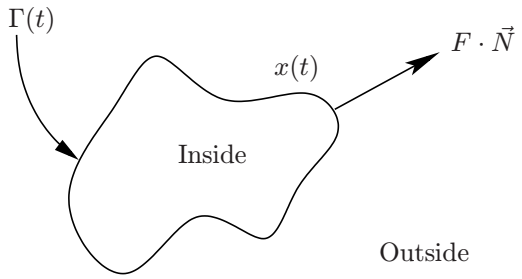

Figure 3: Curve ($\Gamma(t)$) propagating with speed (F) in normal direction ($\vec{N}$).

topological changes in $\Gamma(t)$ are handled naturally. Moreover, normals, curvatures and other properties of the evolving front can easily be computed from $\phi(t)$.

In order to properly capture the vessel boundaries, an approximate speed function F needs to be selected. At the risk of laboring the obvious, we emphasize that segmentations are derived from the steady-state datasets, and therefore the speed functions are derived from these steady-state data as well.

2.3.2. Artery-Vein Separation using Level-Sets: Speed Function

In level-set based segmentation, the speed of the evolving front is given by the speed function F, see Equation 14, which is based on image information. For this application the influence of four speed terms was investigated.

The first component of the speed term, F_{int}, is based on zeroth-order (*i.e.* grey-level) information. The histogram of the CE-MRA dataset shows two distinct peaks, representing the background and the vasculature, respectively. Two normal distributions were fitted to the histogram of the dataset using the expectation max-

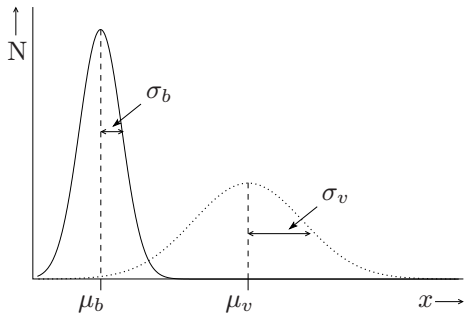

Figure 4. Histogram of contrast-enhanced MR images of the vasculature. The background and the vasculature are characterized by the normal distributions $\mathcal{N}(\mu_b, \sigma_b)$ and $\mathcal{N}(\mu_v, \sigma_v)$, respectively.

imization algorithm.[27] The distributions of the background and the vasculature are described by $\mathcal{N}(\mu_b, \sigma_b)$ and $\mathcal{N}(\mu_v, \sigma_v)$, respectively. Since in CE-MRA vessels give higher signal than the background, it is clear that $\mu_v > \mu_b$. Based on these parameters, the grey-level based speed term is defined as:

$$F_{int}(x) = \frac{1}{\sigma_v\sqrt{2\pi}} \int_0^x e^{-\frac{1}{2}(\frac{x-\mu_v}{\sigma_v})^2} dx, \tag{15}$$

where x is the image grey-value. Note that with this approach no ad hoc threshold parameter is selected as it is derived from image information.

The second component of the speed term, F_{grad}, is based on first-order (*i.e.* gradient) information. The gradient image is calculated by convolving the steady-state dataset with the first-order derivative of the Gaussian kernel. Since the Gaussian filter is an isotropic operator, the data are smoothed in all directions, including object

boundaries. Consequently, the gradient image needs to be calculated at a small scale. The gradient-based speed function is given by:

$$F_{grad}(x) = e^{-\frac{1}{2}(\frac{\nabla I(x)}{C_{grad}})^2}, \tag{16}$$

resulting in low speed values near the object boundary, and large values elsewhere. C_{grad} tunes the gradient. One should realize that the speed term outside the object boundaries has the same positive value as inside the object boundaries. If the evolving front leaks through the object boundaries, it will evolve unboundedly. C_{grad} is a parameter which should be tuned as it is not automatically determined in the current implementation.

The third speed term, F_{vessel}, equals the vesselness function (Equation 9). So, the vesselness-based speed term is defined by:

$$F_{vessel}(x) = \mathcal{V}(x). \tag{17}$$

This value is high at the center of the vesssel and low at the boundary. Disadvantage of this speed function is that it falls short if the assumption of tubular structures no longer holds, *e.g.* at the height of bifuractions.

The last speed term, F_{scale}, that was tested is based on scale-information. The scale-information is derived from the vessel-enhancement filtering process (see Equation 9). The value of each voxel in the scale-image corresponds to the scale at which the output of the vessel-enhancement filtering proces is maximal . This scale is an indication for the local vessel-width. Using the scale-information, a speed image can be made that aims to evolve the front so as to arrive at the vessel boundaries at the same time regardless the vessel-width. This is illustrated in Figure 5. The scale-based speed term is defined as:

$$F_{scale}(x) = \frac{\mathcal{S}(x)}{\mathcal{S}_{max}} e^{-\frac{1}{2}(\frac{d(x)}{\mathcal{S}(x)})^2}. \tag{18}$$

Here denotes $d(x)$ the smallest Euclidean distance of each voxel to the CA, and $\mathcal{S}_{max}$ is the maximum occuring scale along the CA. $\mathcal{S}(x)$ denotes the scale at position x found by blurring the scales along the CA.

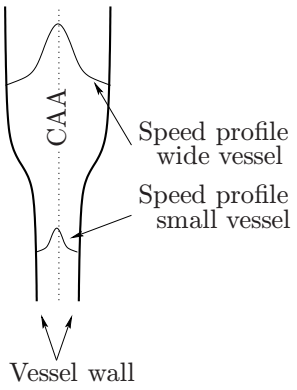

Figure 5: The evolving front arrives at the same time regardless the vessel-width.

Since the separate terms of the speed function have different properties, the applied speed function F is composed by multiplying one or more of these speed terms:

$$F = F_{int} \cdot F_{grad} \cdot F_{vessel} \cdot F_{scale}, \tag{19}$$

where a speed term is equal to 1 if it is not included. All speed terms are normalized, so values are in the range $[0, 1]$.

To ensure the complete segmentation of the vasculature, we *over*segmented both the arterial and venous part of the vasculature. In order to select whether a voxel is part of the arterial or venous the vasculature, the passage-time of the zero level-set for each voxel is registered. Two level-sets are propagated, one starting from the CAA and the other from the CVA. It is to be expected that the passage-time of the zero level-set for a voxel belonging to the arterial (venous) part of the vasculature is smaller for the evolution starting from the CAA (CVA) than starting from the CVA (CAA). So, voxels are labeled arterial or venous based on the arrival time of the respective front.

3. EXPERIMENTS

The described techniques have been applied to six CE-MRA datasets (NC100150, Nycomed Imaging AS, Oslo, Norway). The cost-function for the semi-automatic path tracking is given by the reciprocal output of the vesselness image. Both the first-pass and steady-state datasets were filtered using the same parameters: 25 scales (exponentially increasing) σ = 0.5 - 15.0 mm, α and β were both fixed at 0.5, while γ equals 25% of the maximum occuring pixel-value in the image (see Equation 8). The obtained paths were smoothed with σ = 3.5 mm. If a first-pass dataset is available, the CAA is derived from it and transferred to the steady-state dataset. The CVA is derived from the steady-state dataset. Axes are determined between user-defined points. For additional branches to the arterial or venous axial tree, two more user-defined points are needed.

Using the CAA in the steady-state data as initialization, a rough segmentation of the arteries (that are seeded by the CAA) is made with the level-set technique as described in Section 2.3. The vessel-enhanced image of the steady-state dataset is applied as the speed function. Equation 14 was implemented using a simple Euler forward-scheme with time-step $\Delta t = 0.1$. After removing the largest part of the arterial vasculature, the CVA is determined using the reciprocal output of the vesselness image of the steady-state dataset.

Once the CAA and CVA are known, the evolution of two level-sets is started with these axes as initializations: one to capture the arterial part and one to capture the venous part of the vasculature, respectively. All speed functions (as discussed in Section 2.3.2) were tested separately using different parameters.

4. RESULTS

To obtain a rough segmentation of the arteries, using the CAA as initialization and the vesselness-based speed term as the applied speed function, the number of required iterations was 100. When suppressing the arteries, the CVA could succesfully be obtained. Once the CAA and CVA are known, arteries and veins are segmented and separated using the level-set based technique. All speed terms were tested separately for artery-vein separation. Since intensity- and gradient-based speed terms worked well, but still in some regions leakage occured, a combination of these two was tested, which yielded the best results. Parameters for the gradient-based speed term were: $\sigma = 0.5$ (in all directions), and $C_{grad} = 64.0$. The scale-based speed term was not used, due to its inaccuracy: if an occlusion occurs, the vesselness filter finds the highest response at the largest scale used in the filtering process, although no vessel structure is present. Consequently, the corresponding speed at the central axis will be large, although it should be zero. Since the vesselness-based speed function falls short if the assumption of tubular structures no longer holds (*e.g.* at the height of bifuractions), this speed term was not used in the applied speed function as well.

With the applied speed function ($F = F_{int} \cdot F_{grad}$), the evolution was terminated after 150 iterations. Figures 6 and 7 illustrate the results of the artery-vein separation.

5. DISCUSSION

Clinical use of BPA CE-MRA is hampered due to simultaneous enhancement of arteries and veins. In order for BPAs to gain clinical acceptance, methods for improved visualization, or artery-vein separation are required. In this paper artery-vein separation based on simultaneously evolving the arterial and venous structures using level-set techniques with the central axes as initialization is proposed.

Since arteries and veins are in close proximity in our application, the success of the procedure strongly depends on initialization accuracy and the discriminating quality of the applied speed function. By using

central vessel axes, a good initialization is guaranteed in our approach. To determine the optimal discriminant function, four speed terms were tested. A combination of intensity and gradient-based speed terms appeared to give the best results in this separation task. With this speed term, we obtained qualitatively good separation of the arteries and veins, which can be used for improved visualization. The user-interaction of the entire procedure is very limited if first-pass images are available to determine the CAA and, thus, an important step towards a quick interpretation of steady-state BPA data.

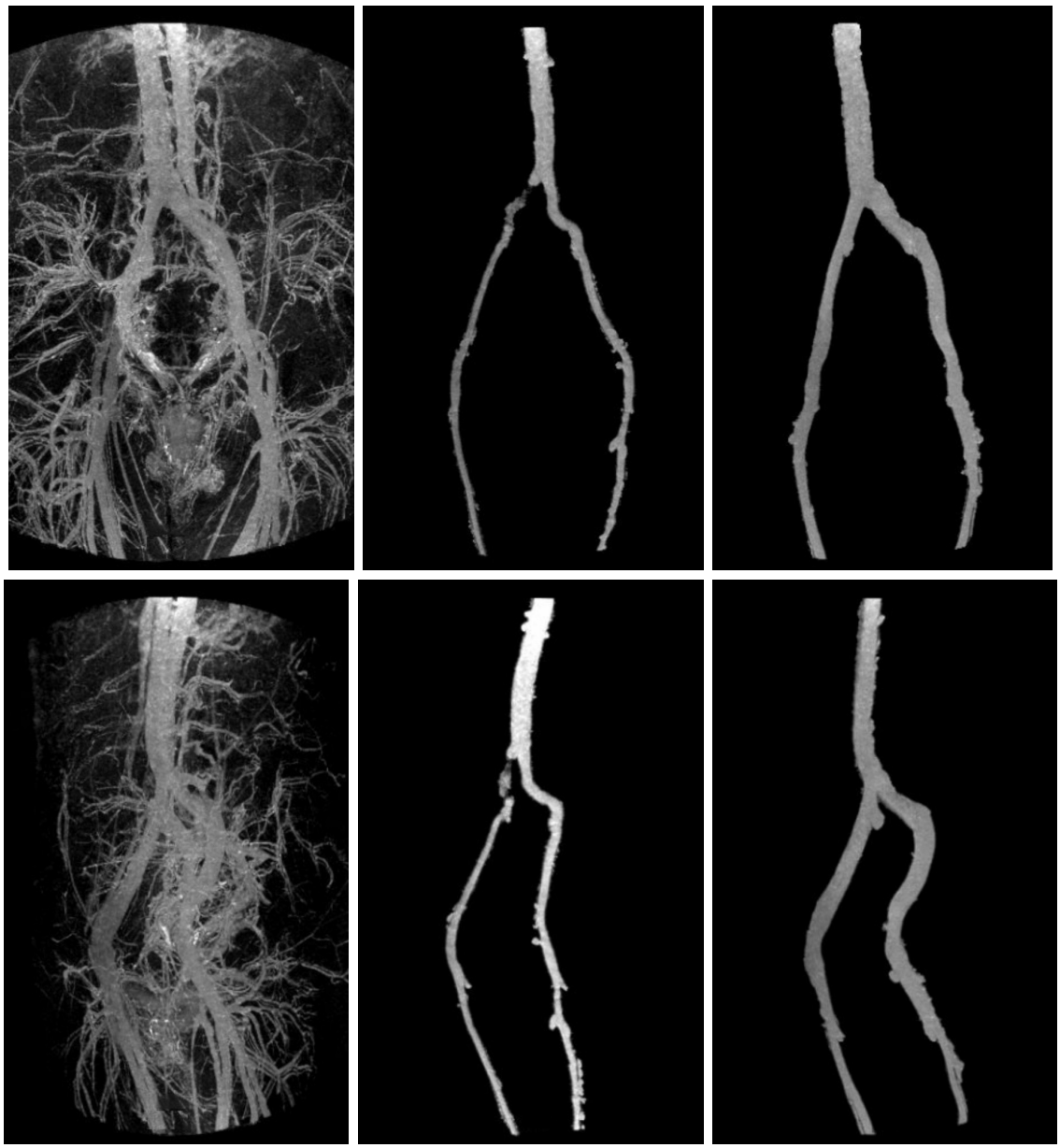

Figure 6. Maximum intensity projection (MIP) of a steady-state dataset. Coronal and oblique views (top and bottom row, respectively) show the complete vasculature, the arterial, and venous part of the vasculature (left, middle, and right column, respectively). In the left image it can be seen that arterial interpretation is hampered without artery-vein separation, whereas after separation a good overview of the main arteries and veins is achieved.

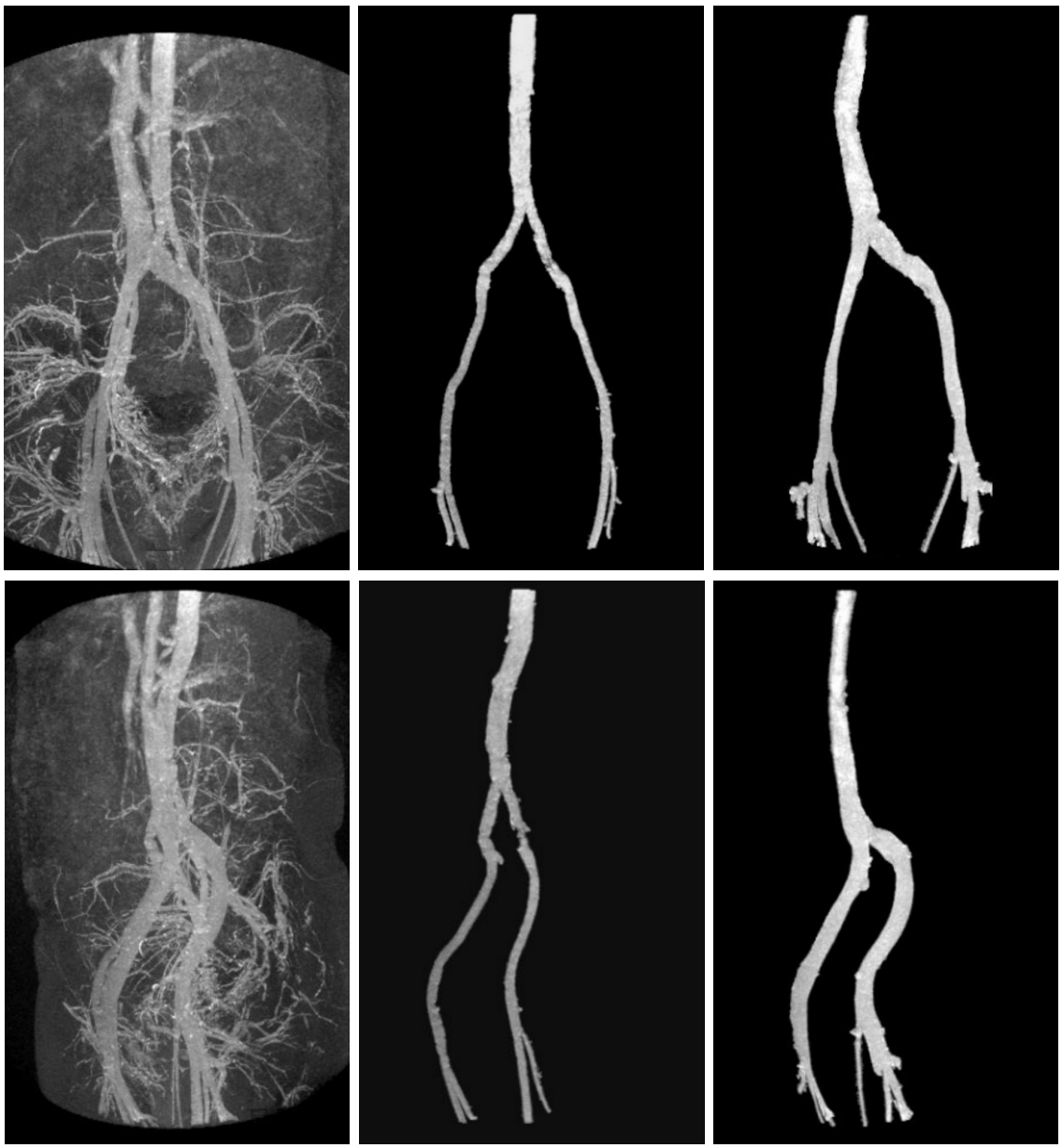

Figure 7. Maximum intensity projection (MIP) of a steady-state dataset. Coronal and oblique views (top and bottom row, respectively) show the complete vasculature, the arterial, and venous part of the vasculature (left, middle, and right column, respectively). In the left image it can be seen that arterial interpretation is hampered without artery-vein separation, whereas after separation a good overview of the main arteries and veins is achieved.

REFERENCES

1. T.M. Grist, F.R. Korosec, D.C. Peters, R.C. Walovitch, R.P. Dolan, W.E. Bridson, and E. C.A. Mistretta, "Steady-State and Dynamic MR Angiography with MS-325: Initial Experience in Humans," *Radiology* **207**, pp. 539–544, 1998.
2. M. Saeed, M.F. Wendland, and C.B. Higgins, "Blood Pool MR Contrast Agents for Cardiovascular Imaging," *JMRI* **12**, pp. 890–898, 2000.
3. D.A. Bluemke, R.D. Darrow, R. Gupta, S.K. Tadikonda, and C.L. Domoulin, "3D Contrast Enhanced Phase Contrast Angiography: Utility for Arterial/Venous Segmentation," in *Proc. ISMRM*, **7**, p. 1237, 1999.
4. T.K.F. Foo, V.B. Ho, M.N. Hood, J.M. Czum, S.D. Wolff, Y. Zhang, and P.L. Choyke, "A Novel Method for MR Arterial and Venous Discrimination Using Gated Phase Contrast and VENC Selection," in *Proc. ISMRM*, **7**, p. 2182, 1999.
5. Y. Wang, Y.Yu, D. Li, K.T. Bae, J.J. Brown, W. Lin, and E.M. Haacke, "Artery and Vein Separation Using Susceptibility-Dependent Phase in Contrast-Enhanced MRA," *JMRI* **12**, pp. 661–670, 2000.
6. Y. Mazaheri, T.J. Carroll, C.A. Mistretta, F.R. Korosec, and T.M. Grist, "Vessel Segmentation in 3D MR Angiography Using Time Resolved Acquistion Curves," in *Proc. ISMRM*, **7**, p. 2181, 1999.
7. S. Aylward, E. Bullitt, S. Pizer, and D. Eberly, "Intensity Ridge and Widths for Tubular Object Segmentation and Description," in *Proc. Workshop on Mathematical Methods in Biomedical Image Analysis*, A. A. Amini and F. L. Bookstein, eds., pp. 131–138, 1996.
8. Th. M. Koller, G. Gerig, G. Székely, and D. Dettwiler, "Multiscale detection of curvilinear structures in 2D and 3D image data," in *Fifth International Conference on Computer Vision*, pp. 864–869, 1995.
9. C. Lorenz, I.-C. Carlsen, T. Buzug, C. Fassnacht, and J. Weese, "Multi-scale Line Segmentation with Automatic Estimation of Width, Contrast and Tangential Direction in 2D and 3D Medical Images," in *Proc. CVRMed and MRCAS*, J. Troccaz, E. Grimson, and R. Mösgez, eds., *Lecture Notes in Computer Science*(1205), pp. 233–242, Springer Verlag, Berlin, 1997.
10. Y. Sato, S. Nakajima, H. Atsumi, T. Koller, G. Gerig, S. Yoshida, and R. Kikinis, "3D Multi-Scale Line Filter for Segmentation and Visualization of Curvilinear Structures in Medical Images," in *Proc. CVRMed and MRCAS*, J. Troccaz, E. Grimson, and R. Mösgez, eds., *Lecture Notes in Computer Science*(1205), pp. 213–222, Springer Verlag, Berlin, 1997.
11. A.F. Frangi, W.J. Niessen, K.L. Vincken, and M.A. Viergever, "Multiscale Vessel Enhancement Filtering," in *Proc. Medical Image Computing and Computer-Assisted Intervention*, W. Wells, A. Colchester, and S. Delp, eds., *Lecture Notes in Computer Science*, pp. 130–137, Springer Verlag, Berlin, 1998.
12. L.M. Lorigo, O. Faugeras, W.E.L. Grimson, R. Keriven, R. Kikinis, A. Nabavi, and C.-F. Westin, "CURVES: Curve Evolution for Vessel Segmentation," *Medical Image Analysis* **5**, pp. 195–206, 2001.
13. I. Nyström and Ö. Smedby, "A New Presentation Method for Magnetic Resonance Angiography Images based on Skeletonization," in *Proc. SPIE*, **3976**, pp. 515–522, 2000.
14. M. Bock, S.O. Schoenberg, F. Floemer, A. Grau, R. Strecker, and L.R. Schad, "Artery-Vein Separation in 3D Contrast Enhanced Pulmonary MRA using Correlation Analysis," *Proc. ISMRM* , p. 486, 1999.
15. W.J. Niessen, A.D. Montauban van Swijndregt, B.H.P. Elsman, O. Wink, W.P.Th. M. Mali, and M.A. Viergever, "Enhanced Artery Visualization in Blood Pool MRA: Results in the Peripheral Vasculature," in *Proc. Medical Image Computing and Computer-Assisted Intervention*, W. Wells, A. Colchester, and S. Delp, eds., *Lecture Notes in Computer Science*, pp. 340–345, Springer Verlag, Berlin, 1998.
16. M. Sonka, R. Stephancik, and S. Tadikonda, "Feasibility of Automated Separation of Arteries and Veins Using a Graph Searching Technique," in *Proc. ISMRM*, **7**, p. 2183, 1999.
17. T. Lei, J.K. Udupa, P.K. Saha, and D. Odhner, "Artery-Vein Separation via MRA - An Image Processing Approach," *IEEE Transactions on Medical Imaging* **20**, pp. 689–703, 2001.
18. J.K. Udupa and S. Samarasekera, "Fuzzy Connectedness and Object Delineation: Theory, Algorithm, and Validation," *Graphical Models and Image Processing* **58**, pp. 246–261, 1996.

19. C.M. van Bemmel, W.J. Niessen, O. Wink, B. Verdonck, and M.A. Viergever, "Blood Pool Agent CE-MRA: Improved Arterial Visualization of the Aortoiliac Vasculature in the Steady-State Using First Pass Data," in *Proc. Medical Image Computing and Computer-Assisted Intervention*, W. Niessen and M. Viergever, eds., *Lecture Notes in Computer Science*(2208), pp. 699–706, Springer Verlag, Berlin, 2001.
20. E. Dijkstra, "A Note on Two Problems in Connexion with Graphs," *Numerische Mathematik* **1**, pp. 269–271, 1959.
21. O. Wink, W.J. Niessen, and M.A. Viergever, "Minimum Cost Path Determination Using a Simple Heuristic Function," in *Proc. International Conference on Pattern Recognition*, A. Sanfelin, J. Villanueva, M. Vanrell, R. Alquézar, T. Huang, and J. Serra, eds., pp. 1010–1013, IEEE Computer Society, Piscataway, NJ, September 2000.
22. W.M. Wells, P. Viola, H. Atsumi, S. Nakajima, and R. Kikinis, "Multi-Modal Volume Registration by Maximization of Mutual Information," *Medical Image Analysis* **1**, pp. 35–51, March 1996.
23. F. Maes, A. Collignon, D. Vandermeulen, G. Marchal, and P. Suetens, "Multimodality Image Registration by Maximization of Mutual Information," *IEEE Transactions on Medical Imaging* **16**, pp. 187–198, 1997.
24. S. Osher and J.A. Sethian, "Fronts Propagating with Curvature Dependent Speed: Algorithms Based on Hamilton-Jacobi Formulations," *Journal of Computational Physics* **79**, pp. 12–49, 1988.
25. J.A. Sethian, "A Review of the Theory, Algorithms, and Applications of Level Set Methods for Propagating Interfaces," *Acta Numerica* **5**, 1996.
26. J.A. Sethian, *Level Set Methods and Fast Marching Methods*, Cambridge University Press, second ed., 1999.
27. C.M. Bishop, *Neural Networks for Pattern Recognition*, Oxford University Press Inc., New York, 1995.